EES Batteries

ROYAL SOCIETY OF CHEMISTRY

PAPER

View Article Online
View Journal | View Issue

Cite this: *EES Batteries*, 2025, **1**, 1245

Dual-function surface–bulk engineering *via* a one-step strategy enables efficient upcycling of degraded NCM523 cathodes†

Ji Shen,‡ Miaomiao Zhou,‡ Wei Liu, Haocheng Pi and Ruiping Liu *

Received 10th May 2025,
Accepted 13th July 2025

DOI: 10.1039/d5eb00090d

rsc.li/EESBatteries

Enhancing the performance of recycled cathodes and improving their market competitiveness against comparable commercial cathode materials remains a fundamental challenge for direct recycling technologies of spent cathodes. Herein, a dual modification strategy incorporating surface coating and bulk doping of cathode materials during the regeneration process of spent cathodes has been implemented to enhance the cycling stability. The composite coating layer consisting of Li_2SO_4, Li_3N, $LiNO_3$, and LiF on the surface of regenerated cathodes facilitates Li^+ transport and mitigates electrolyte-induced cathode material degradation. F doping facilitates the formation of F–Ni bonds, which effectively suppresses the oxidation of Ni^{2+} to Ni^{3+}, thereby enhancing the regeneration efficiency of spent cathodes while reducing the formation of detrimental spinel and rock-salt phases. N doping generates strong N–O bonds that effectively immobilize lattice oxygen, thereby stabilizing the crystal structure. The upcycled cathode demonstrates superior electrochemical performance, achieving a discharge specific capacity of 168.8 mAh g^{-1} at 0.1C and the capacity retention is 77.1% after 200 cycles at 0.5C. This study holds significant importance for upcycling spent cathodes into fully healthy cathodes with long-life characteristics.

Broader context

The research on cycling of spent Li-ion battery cathodes is currently an important and hot topic. Issues include the cathode failure mechanism and performance enhancement of spent cathodes. Nevertheless, traditional direct regeneration techniques predominantly concentrate on lithium supplementation, with regenerated cathode performance generally approximating that of commercial cathodes, and the market competitiveness with commercial cathodes is not obvious. We firmly believe that this original work would draw considerable attention from a broad range of readers from interdisciplinary fields, including cathode preparation, failure mechanism study, spent cathode regeneration, *etc*.

1. Introduction

The demand for lithium-ion batteries (LIBs) is exploding as the market for electric vehicles (EVs) is expanding.[1,2] $LiNi_{0.5}Co_{0.2}Mn_{0.3}O_2$ (NCM) is widely used in LIB cathodes, owing to its balanced performance in terms of energy density and cycling stability. The extensive use of LIBs and their limited 8-year life cycle is expected to generate a large number of spent LIBs in the future.[3] The spent LIBs harbor metal resources and toxic substances that, if improperly disposed of, can lead to significant resource wastage and environmental pollution.[4] Hence, to prevent the emergence of resource and environmental crises, it is imperative to prioritize the proper handling and utilization of spent LIBs.

Presently, to better address the challenges of recycling spent lithium-ion batteries, researchers have proposed a direct recycling process that offers the advantages of being non-destructive and capable of *in situ* regeneration. As a result, direct recycling is considered the next-generation recycling technology for LIBs.[5] A range of feasible direct recovery methods have been introduced, including solid-phase,[6] hydrothermal,[7] eutectic salt,[8,9] electrochemical,[10] and chemical lithiation processes.[11] The solid-phase method represents a straightforward and effective regeneration approach, accomplished by blending a specified amount of lithium salts (LiOH, Li_2CO_3) with spent $LiNi_{0.5}Co_{0.2}Mn_{0.3}O_2$ (S-NCM), followed by sintering to facilitate elemental replenishment and structural repair of the S-NCM. Nevertheless, traditional solid-phase techniques predominantly concentrate on lithium supplementation, with regenerated cathode performance generally

School of Chemical & Environmental Engineering, China University of Mining & Technology (Beijing), Beijing, 100083, PR China. E-mail: 201402@cumtb.edu.cn

†Electronic supplementary information (ESI) available. See DOI: https://doi.org/10.1039/d5eb00090d

‡These authors contributed equally to this work.

approximating that of commercial cathodes.[12,13] Thus, integrating cathode modification technology with the solid-phase method to elevate the performance of the regenerated cathode and achieve the upcycling of S-NCM holds significant prospects for wide-ranging applications.

While NCM exhibits excellent performance in terms of energy density and cycling stability, it experiences irreversible lithium loss after deep discharge and prolonged charge/discharge cycling, leading to structural collapse of the NCM layered structure and consequent capacity degradation.[14,15] Moreover, the Ni element in the NCM is readily oxidized through side reactions with the electrolyte, resulting in the formation of a Ni-rich surface oxide layer. The oxide layer consists of oxides such as NiO_2, where Ni is mainly present in the form of Ni^{3+}.[16] For the failure of transition metal layered oxides, the escape of lattice oxygen is also a key contributing factor to the degradation of NCM materials, which will lead to the instability of the crystal structure and capacity decay of NCM.[17]

Herein, targeting the common failure mechanism of NCM, we propose a simple solid-phase sintering method for the upcycling of S-NCM materials. First, Li_2CO_3 is utilized as a lithium source to replenish lithium and repair structural defects in S-NCM. Subsequently, to address the challenges of easy generation of impurities at the NCM surface and the escape of lattice oxygen caused by electrolyte side reactions, we achieved dual modification by coating and doping regenerated S-NCM using commonly available lithium bis(trifluoromethanesulfonimide) (LiTFSI) as a bifunctional coating agent and dopant. LiTFSI is abundant in F, N, and S elements. During the regeneration process, Li_2SO_4, Li_3N, $LiNO_3$, and LiF composite coatings are generated on the surface of upcycled NCM (U-NCM). In addition to the surface coating modification, the N element is successfully doped into the Li–O sheet layer, forming N–O bonds to fix the lattice oxygen and reduce oxygen loss. Simultaneously, F occupies some of the O sites to form Ni–F bonds, which reduces the oxidation state of the Ni element and inhibits the formation of NiO_2 oxides from Ni^{3+}.[18] The U-NCM exhibits a discharge specific capacity of 168.8 mAh g^{-1} at 0.1C and capacity retention of 77.1% after 200 cycles at 0.5C. This work may provide a simple novel method for upcycling cathodes.

2. Results and discussion

2.1. Mechanism of upcycling NCM

As shown in Fig. 1, the life cycle of LIBs and the mechanism of S-NCM upcycling are briefly demonstrated. The unused commercial NCM cathode retains its layered structure, with Li atoms, O atoms, and transition metal atoms being orderly arranged. After extended use in electrical devices such as electric vehicles, NCM experiences structural damage and significant capacity degradation due to the irreversible loss of Li^+ and the release of lattice oxygen in the form of O_2.[19,20] Moreover, prolonged contact between the cathode and the electrolyte leads to the occurrence of side reactions, during which Ni^{2+} is oxidized to Ni^{3+}, forming NiO_2. This process consumes the electrolyte and produces electrochemically inert impurities, which further contribute to the loss of capacity and structural degradation of the NCM, transforming it into S-NCM.[21] Due to the incorporation of LiTFSI, after the repair process, Li_2SO_4, Li_3N, $LiNO_3$, and LiF coatings are simultaneously generated on the U-NCM surface along with re-lithiation and structural repair. S, N, and F elements further diffuse into the interior of the material to achieve elemental doping of the NCM.

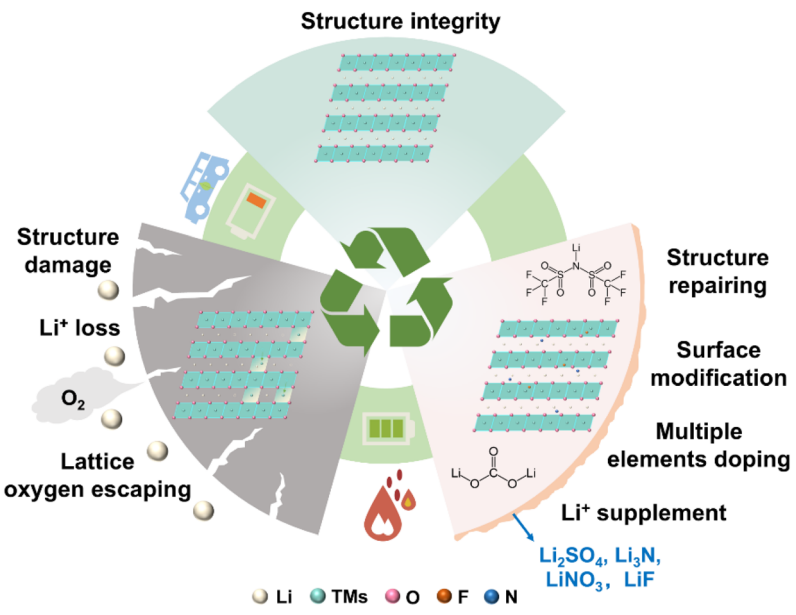

Fig. 1 Schematic illustration of the upcycling procedure of S-NCM cathodes.

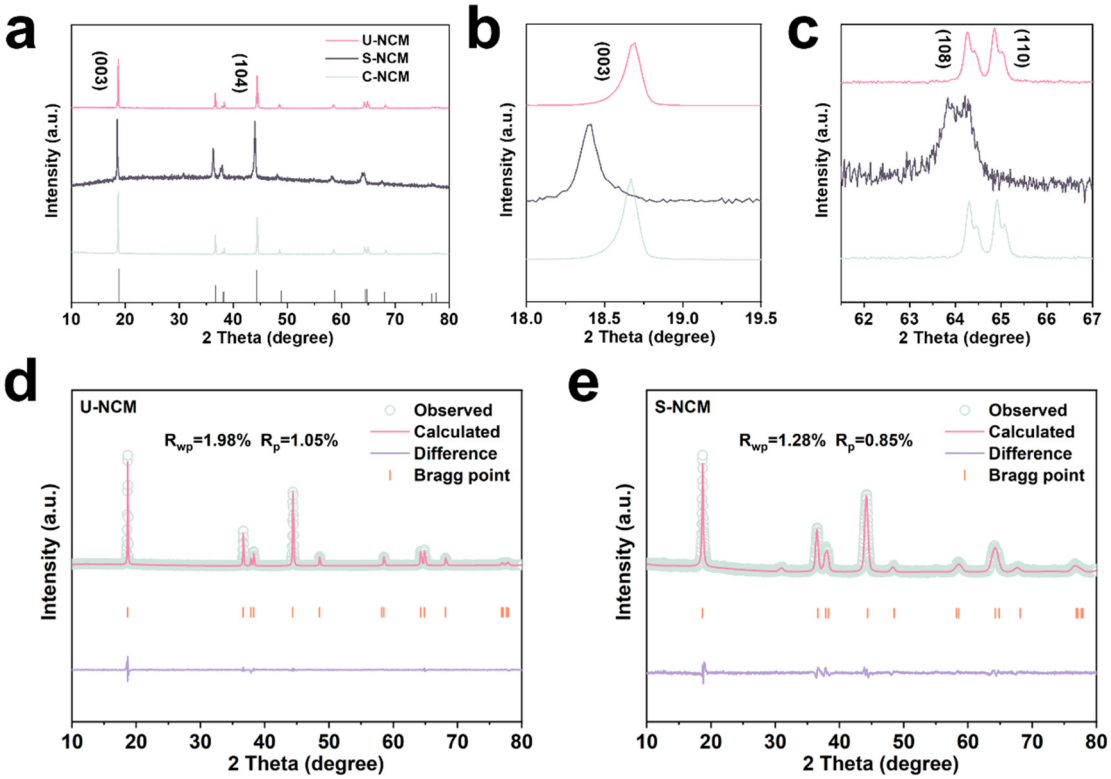

Fig. 2 (a–c) XRD patterns and partially enlarged details of U-NCM, S-NCM and C-NCM. (d and e) Rietveld refinements of XRD patterns of U-NCM and S-NCM.

In order to verify the effectiveness of the cathode regeneration process, X-ray diffraction (XRD) characterization was carried out to reveal the structural difference between U-NCM, S-NCM and C-NCM. As shown in Fig. 2a, all diffraction peaks of the three samples correspond to the $R\bar{3}m$ symmetric space group structure. Among these samples, the diffraction peaks of S-NCM differ significantly from those of the other two samples. Specifically, the (003) peak of S-NCM exhibits relatively low intensity, while the (104) peak shows higher intensity. The $I_{(003)}/I_{(104)}$ peak ratio indicates the Li/Ni disorder in NCM.[22] S-NCM exhibits the lowest $I_{(003)}/I_{(104)}$ ratio, signifying a higher degree of Li/Ni disorder. Li/Ni disorder arises from the migration of Ni atoms into lower energy Li vacancies.[23] The migration of Ni atoms to Li vacancies obstructs the one-dimensional diffusion channel for Li^+, impeding Li^+ transport and resulting in the degradation of electrochemical performance. Fig. 2b and c show the locally enlarged views of the (003), (108), and (110) peaks. It is evident that the (003) peak of S-NCM is shifted to a lower angle. This is ascribed to the significant amount of Li^+ deficiency in S-NCM, which results in increased electrostatic repulsion between the transition metal layers and triggers the expansion of the crystal along the *c*-axis direction. After regeneration, the (003) peak of U-NCM is restored to the same position as that of C-NCM, proving that the proposed regeneration strategy achieves lithium replenishment and restores the layered structure for S-NCM. Another noticeable difference is between the (108) and (110) split peaks. The (108) and (110) peaks of S-NCM do not exhibit splitting, suggesting that its layered structure has been damaged. In contrast, U-NCM and C-NCM display distinct (108) and (110) splitting peaks, indicating a well-ordered layered structure.[22] Furthermore, the sharper diffraction peaks of U-NCM and C-NCM indicate that U-NCM and C-NCM possess higher crystallinity. In order to explore the influence of different addition amounts of LTFSI on the structure of the regenerated cathode, we carried out XRD analyses on different samples. As shown in Fig. 2a and S2,† U-NCM, U-NCM-0, U-NCM-1 and U-NCM-2 are regenerated with S-NCM incorporated with 0.025 g, 0 g, 0.0125 g and 0.0375 g LiTFSI, respectively, and the crystal structures of the samples with different addition amounts of LiTFSI are the same and exhibit the $R\bar{3}m$ symmetric space group structure. This indicates that the addition of LiTFSI cannot change the structure of the NCM cathode.

As shown in Fig. 2d–e and Fig. S1,† the Rietveld refinement models for U-NCM, S-NCM, and C-NCM provide a detailed depiction of the lattice parameter variations and the extent of cation mixing. As shown in Table S3,† the S-NCM exhibits a significant Li/Ni inversion ratio of 18.8% due to the loss of Li-ions. Furthermore, the crystal expands along the *c*-axis, with the *c*-parameter rising to 14.3531 Å, which is higher than that of the upcycled cathode U-NCM (4.2% and 14.2470 Å) and the commercial cathode C-NCM (5.8% and 14.2364 Å) (Tables S2–S4†). The results all demonstrate that the U-NCM restores the layered structure, which is in agreement with the XRD conclusions mentioned above.

The morphologies of S-NCM and U-NCM were directly observed using scanning electron microscopy (SEM). S-NCM exhibits a spherical polycrystalline structure, characterized by the agglomeration of small particles on its surface, which appears relatively loose and riddled with numerous voids. This condition might stem from the cycling stress and strain induced in the NCM during extended cycling, potentially resulting in the shedding of small particles from the cathode (Fig. 3a). The magnified image of region I reveals in detail the poor surface conditions of S-NCM, where cracks, fragments and holes are present on the particle surface. Cracks and fragmentation may result from cycling stress induced by the lattice expansion and contraction of the cathode during lithium de-intercalation. Additionally, the holes might be attributed to the corrosive effect of the electrolyte on the cathode surface. In contrast, U-NCM exhibits a spherical state characterized by the aggregation of small particles, but notably presents a clean, flat, and smooth surface, which resembles that of the commercial cathode material C-NCM (Fig. 3b and S8†). In addition, the surfaces of U-NCM-1 and U-NCM-2 also exhibit a smooth morphology. In contrast, due to the lack of LiTFSI addition, U-NCM-0 has residual excess lithium salts on its surface, presenting a rough surface (Fig. S9–11†). Based on the comparison of the morphological features of S-NCM and U-NCM cathode materials, it is evident that following upcycling, the structural defects inherent in S-NCM are effectively eradicated.

To explore the underlying mechanism of cathode material regeneration, the samples were subjected to high-resolution transmission electron microscopy (HRTEM) analysis. For S-NCM, the rock salt phase, spinel phase and layered phase are present within the material particles (Fig. 3c). Both the rock salt and spinel phases are indicative of typical impurity phases due to the migration of transition metal atoms to Li sites.[24] The enlargement of regions II and III, situated near the surface of S-NCM particles, respectively, reveals disordered spinel and rock salt phases. As lithium deficiency progresses from the surface of the material towards its inner bulk, an intact layered structure persists deep within the S-NCM. The lattice spacing in region II for the spinel phase is 0.149 nm. The spacing is smaller than the adjacent facet spacing of the normal layered structure, a result of the transition metal occupying the lithium sites.[8] In the HRTEM image of the U-NCM, it is evident that there is a coating layer with a thickness of approximately 2 nm on the surface of the material, which exhibits lattice stripes distinct from those found within the U-NCM, confirming the presence of a crystalline coating layer on the surface of the U-NCM (Fig. 3d). Subsequent XPS (X-ray photoelectron spectroscopy) tests have confirmed that the surface coating is a mixture of Li_2SO_4, $LiNO_3$, Li_3N, and LiF. Moreover, the U-NCM exhibits an ordered and uniform layered structure extending from its surface to the bulk. The inverse Fourier transform and lattice spacing measurements of region

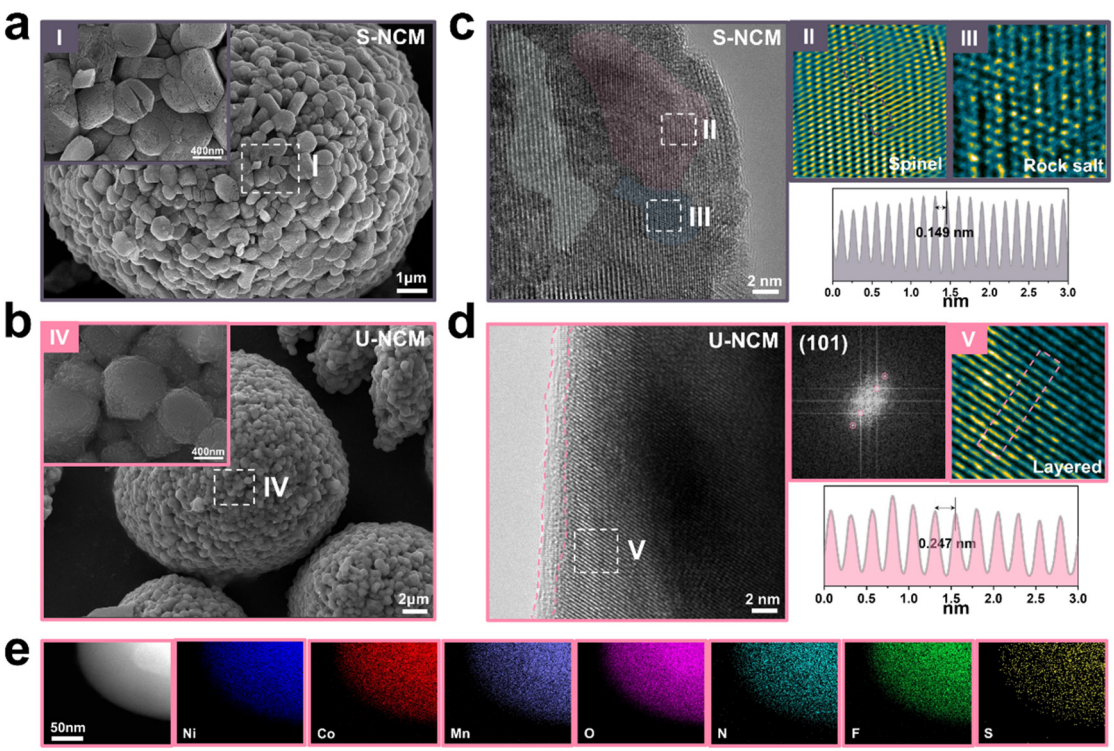

Fig. 3 (a and b) SEM images of S-NCM and U-NCM. Part I and part IV are the enlarged images of the corresponding areas in S-NCM and U-NCM. (c) HRTEM image of S-NCM. Part II and part III are the inverse FFT images of the corresponding areas in S-NCM. (d) HRTEM image of U-NCM. Part V is the inverse FFT image of the corresponding area in U-NCM. (e) STEM of U-NCM with the EDS mapping distribution of Ni, Co, Mn, O, N, F and S elements.

V verify that region V corresponds to the (101) crystalline plane. Random energy dispersive X-ray spectroscopy (EDXS) tests were conducted on the U-NCM, revealing that in addition to the uniform distribution of Ni, Co, Mn, and O elements, the N, F, and S elements employed for doping and coating are also uniformly distributed across the U-NCM particles (Fig. 3e). Using SEM and HRTEM characterization tests, it is shown that after straightforward regeneration operation, defects such as cracks, holes, and the CEI on the surface of S-NCM can be eliminated by recrystallization occurring under high-temperature annealing. Moreover, in a lithium-rich environment provided by Li_2CO_3, the spinel phase and the rock salt phase are transformed into a layered structure.

X-ray photoelectron spectroscopy (XPS) was used to explore the upcycling effect on S-NCM, U-NCM, and C-NCM. The characteristic Ni element in ternary layered cathode materials is characterized. For NCM cathodes, nickel typically exists in a mixed valence state, combining both +2 and +3 valences.[25] When irreversible lithium loss occurs at the NCM cathode, to maintain the charge balance of the material, the valence state of the nickel element is elevated, resulting in a decrease in the Ni^{2+} content and an increase in the Ni^{3+} content.[24] It is therefore possible to assess the state of the cathode material based on the relative proportions of the different valence states of Ni. As shown in Fig. 4a, the unused C-NCM exhibits a higher Ni^{2+} content in the Ni 2p spectra, indicating that the C-NCM is in a healthy state. After electrochemical cycling, the Ni^{2+} ratio in S-NCM decreases, while the Ni^{3+} ratio increases, attributable to the deficit of Li^+ in S-NCM. Furthermore, Ni^{3+} is also a constituent of the electrochemically inert impurity rich spinel and rock salt phases. The S-NCM is found to be in a degraded state based on the Ni 2p spectra. After the S-NCM is repaired, the Ni^{3+} content in the U-NCM decreases, and the Ni^{2+} content increases, aligning with the characteristics of the C-NCM in a healthy state. After lithium supplementation and high-temperature annealing, Li^+ enters the Li sites, transforming Ni^{3+} into Ni^{2+}. Simultaneously, the spinel and rock salt phases transition into layered structures, and the reduction of impurity phases contributes to a decrease in Ni^{3+} and an increase in Ni^{2+}. Another notable element that is sensitive to the state of health of the NCM cathode is O. Prolonged electrochemical cycling of the NCM cathode leads to lattice oxygen deficiency and the release of the O element in the form of oxygen, contributing to the formation of structural defects.[26] As shown in Fig. 4b, the O peaks of all three samples can be fitted into lattice O, TM-O representing the spinel and rock salt phases, and C=O representing surface impurities, primarily from Li_2CO_3. The distinction lies in the relative quantities of O chemical states among the three samples. Notably, a significant amount of TM-O and relatively more C=O are detected in

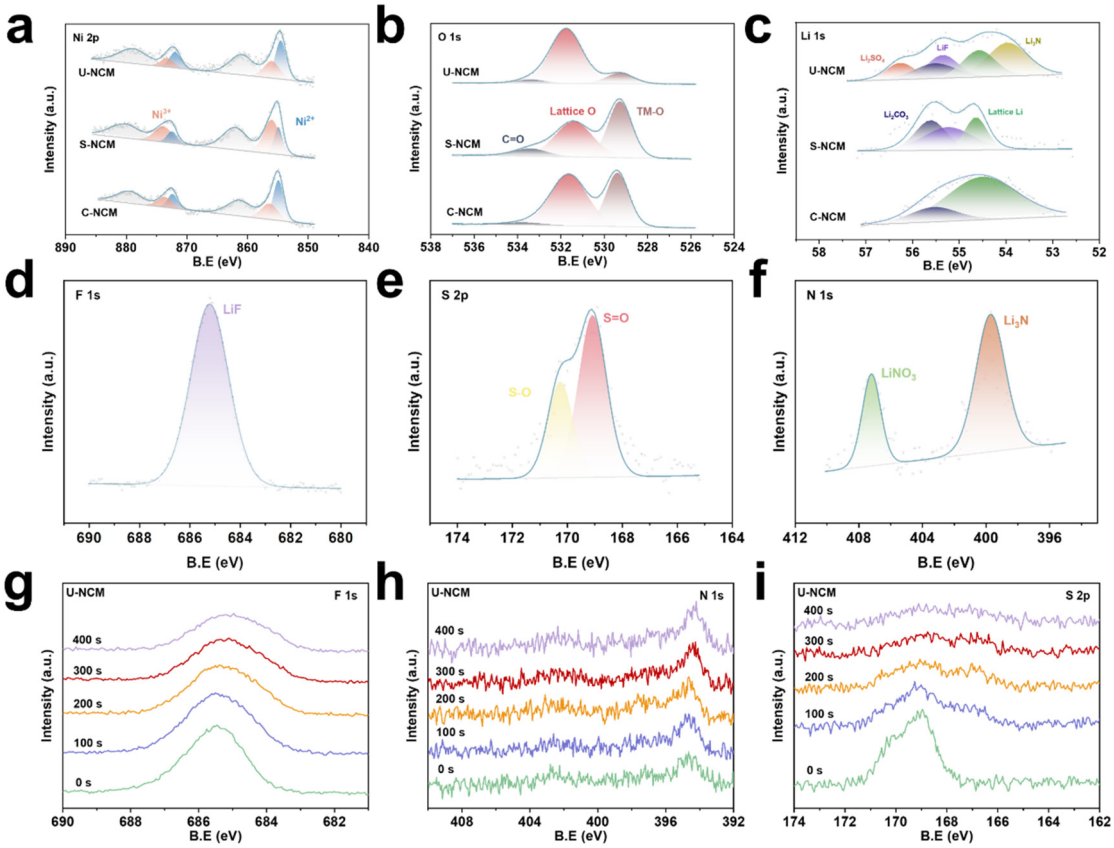

Fig. 4 (a and c) XPS spectra of Ni 2p, O 1s and Li 1s in U-NCM, S-NCM and C-NCM. (d–f) XPS spectra of F 1s, S 2p and N 1s in U-NCM. (g–i) Etching XPS spectra of F 1s, N 1s and S 2p in U-NCM with increasing Ar^+ etching time up to 400 s.

S-NCM, attributable to its degraded state, accompanied by a lower level of lattice oxygen. The restoration of U-NCM from the failed state to the healthy state can be manifested by increased lattice oxygen and reduced TM-O and C=O, indicating that the oxygen defects in S-NCM are repaired. From the above XPS characterization, as well as SEM and HRTEM analyses, it is evident that following the regeneration process, the chemical states of Ni and O are reset to a state nearly identical to that of C-NCM, with structural defects eliminated. In addition, the XPS spectra of Co and Ni elements of U-NCM, S-NCM and C-NCM are shown in Fig. S5 and S6.† The chemical state of the Co element remains essentially unaltered across all samples. Nevertheless, a minute quantity of Mn^{3+} is identified in S-NCM, which can be attributed to the alteration in the charge state due to the loss of O during high-voltage electrochemical cycling.[24] For U-NCM, due to the restoration of lattice oxygen, the charge state of the Mn element is likewise restored, with Mn^{3+} transformed into Mn^{4+}.

To thoroughly investigate the surface coating layer and internal doping of the U-NCM material, XPS characterization was conducted to characterize the elements. As shown in Fig. 4c, the Li 1s spectra of C-NCM exhibit a limited variety of Li elemental chemical states, only the lattice lithium of the material itself and Li_2CO_3. The latter is formed from residual lithium on the surface during the preparation of C-NCM, as well as from the reaction of the surface of the material with H_2O and CO_2 during the storage process.[27] In comparison with C-NCM, S-NCM experiences irreversible Li deficiency, leading to a reduction in lattice lithium content and an increase in Li_2CO_3. The increase in Li_2CO_3 content primarily arises from the side reaction between the cathode material and the electrolyte, resulting in the generation of a CEI, where Li_2CO_3 serves as a common component.[28] Furthermore, the emergence of LiF can also be attributed to the presence of the CEI. The Li element's chemical state in the U-NCM appears to be more complex, featuring the presence of not only lattice lithium and residual Li_2CO_3, but also Li_2SO_4, Li_3N, and LiF. Notably, the LiF on the U-NCM surface does not originate from the CEI but rather constitutes an integral component of the artificial surface coating layer. The XPS result validates that the upcycling strategy effectively achieves a composite coating on the surface of the regenerated material. Separate analytical characterization of the F, S, and N elements within the U-NCM was also conducted (Fig. 4d–f). The emergence of obvious LiF peaks in the F 1s spectra of U-NCM again proves the existence of a LiF coating layer on the surface of U-NCM (Fig. 4d). Additionally, the S 2p pattern exhibits two fitted peaks, S–O and S=O, both of which belong to SO_4^{2-}, affirming the successful formation of a Li_2SO_4 coating layer on the surface of U-NCM (Fig. 4e). The presence of both $LiNO_3$ and Li_3N is also detected on the surface of U-NCM (Fig. 4f). The Li-rich cathode coatings enhance the Li^+ transport between the cathode and the electrolyte, thereby improving the electrical conductivity of the cathode and consequently exhibiting superior electrochemical performance.[29–31] Furthermore, the coating layer on the surface of the cathodes serves as a protective armor for the cathode material, minimizing direct contact between the cathode and the electrolyte, which mitigates side reactions, decreases the consumption of activated lithium and electrolyte, and limits the formation of impurity phases. These attributes collectively enhance the cycling stability of the cathode material.

Etching XPS is commonly employed to investigate the elements within a material, serving as a technique that can characterize the interior of the material. Here, the doping of U-NCM was investigated by sampling the U-NCM every 100 seconds of etching using etching XPS. First, as shown in Fig. 4g, the intensity of the F element signal peak remains nearly unchanged from the initial sampling at the material surface at 0 seconds to the sampling at the 400th second of etching. This indicates that the F element not only forms LiF on the surface of the material but also uniformly distributes throughout the U-NCM, thereby facilitating F element doping. It is worth noting that with increasing etching depth, the signal peak energy of the F element shifts towards lower energies, which is attributed to the formation of F–Ni.[32] The doping of the F element can reduce the chemical state of the Ni element, thereby promoting the transformation of Ni^{3+} to Ni^{2+} during the regeneration process and improving the efficiency of cathode repair. Furthermore, it also inhibits the formation of spinel/rock salt phase impurities in the cathode, thereby enhancing its electrochemical performance. The signal peaks of N elements remain nearly unchanged over the etching time, confirming that the N element is uniformly distributed throughout the U-NCM. This indicates the successful realization of N element doping and the formation of strong N–O bonds (Fig. 4h). A strong S 2p signal peak is measured during the U-NCM surface sampling at 0 seconds, which progressively weakens with increasing etching time (Fig. 4i). The results indicate that the S element only forms a Li_2SO_4 coating layer on the surface of U-NCM and does not diffuse into the material to induce S element doping. The etching XPS test results provide further evidence that the proposed strategy can effectively achieve recycling of S-NCM. The U-NCM obtained features F, N, and S elemental coating layers on its surface, while internally, F–Ni and strong N–O bonds are formed to inhibit the oxidation of nickel ions and the release of lattice oxygen. The dual-strategy modification, achieved through both coating and doping, is expected to endow U-NCM with enhanced electrochemical performance and cycling stability.

2.2. Electrochemical performance of NCM cathodes

The half-cells were assembled, and the electrochemical properties of the cathode materials were evaluated to verify the advantages of the U-NCM cathodes. As shown in Fig. S13† and Fig. 5a, in the initial capacity test, the U-NCM has the highest discharge specific capacity of 168.8 mAh g^{-1}, which has reached the standard of the commercial cathode C-NCM (165.4 mAh g^{-1}). Conversely, the initial discharge specific capacities of the materials without doping and coating (U-NCM-0), with minimal (U-NCM-1) and excessive (U-NCM-2) doping and coating drop to 161.2 mAh g^{-1}, 155.9 mAh g^{-1} and

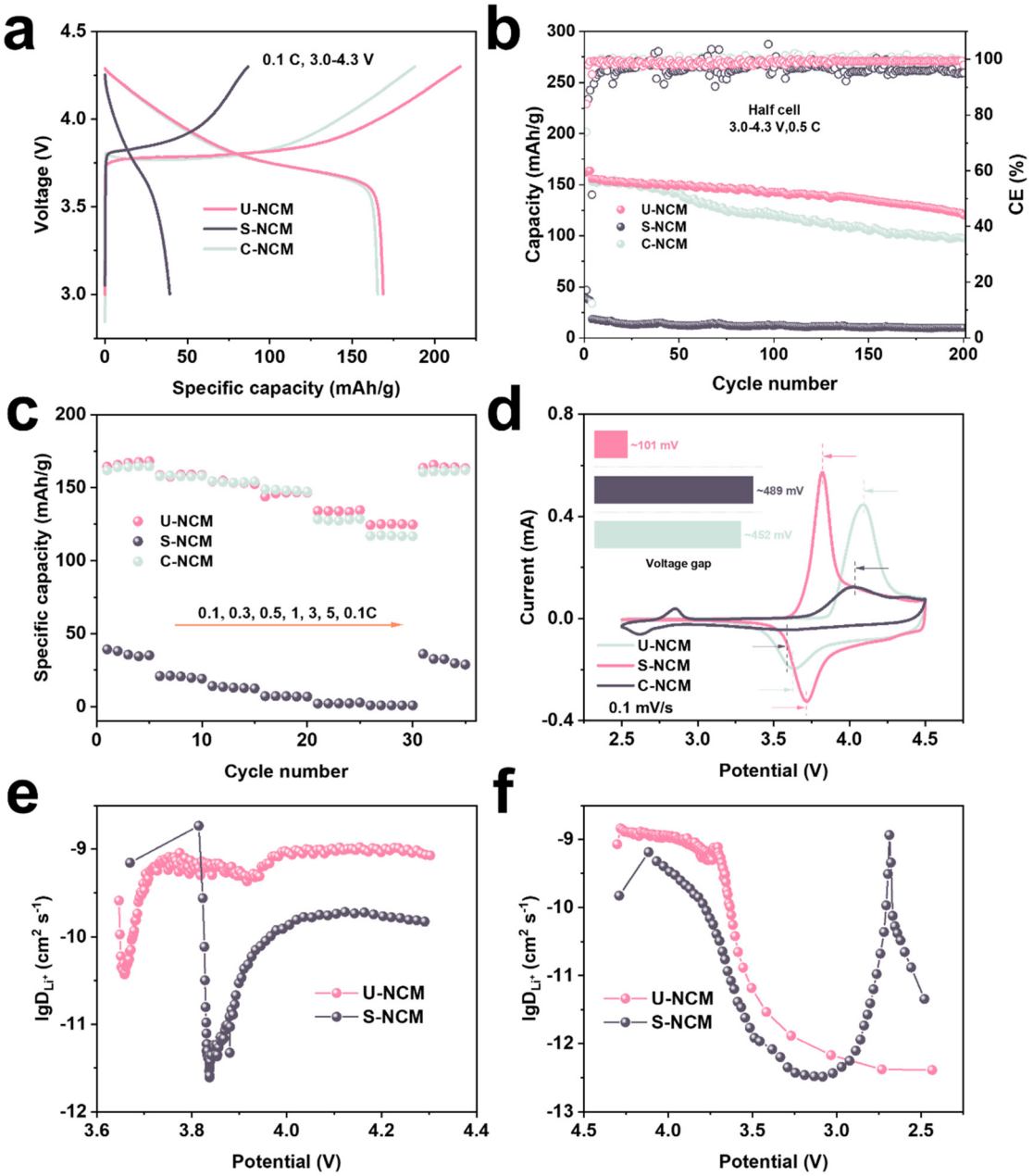

Fig. 5 (a) The charge–discharge curves of cycling tests between 3 and 4.3 V of U-NCM, S-NCM and C-NCM at 0.1C in the first cycle. (b) Cycling performance at 0.5C of U-NCM, S-NCM and C-NCM. (c) Rate performance of U-NCM, S-NCM and C-NCM. (d) CV curves of U-NCM, S-NCM and C-NCM at a scan rate of 0.1 mV s^{-1}. (e and f) GITT results of U-NCM and S-NCM.

145.7 mAh g^{-1}, respectively. This decline might be due to both the inappropriate modification caused by excessive or insufficient quantities of doping and coating agents and the presence of the agents as inactive impurities, which hampers the electrochemical performance of the cathode.[33] Expectedly, the capacity of the S-NCM is found to be below 50 mAh g^{-1}, indicating a failed state. The cycling stability of U-NCM-0, U-NCM-1 and U-NCM-2 is proved to be unsatisfactory as well, exhibiting accelerated decay of the discharge specific capacity after 50 cycles at 0.5C (Fig. S14†). Compared with C-NCM and S-NCM, U-NCM shows excellent cycling stability at 0.5C. The specific capacity of discharge after 100 cycles is 142.9 mAh g^{-1} with a capacity retention of 91.8%, and the capacity retention rate after 200 cycles is 77.1%. The cycling stability of the commercial C-NCM is not as good as that of U-NCM, with the discharge specific capacity dropping to 97.5 mAh g^{-1} after 200 cycles, and the capacity retention rate is only 63.8% (Fig. 5b). Thanks to the coating layer formed on the surface of U-NCM, the side reactions between the cathode and electrolyte are suppressed, resulting in a reduction of active lithium loss and

impurity phase generation. Consequently, the U-NCM can maintain a high reversible specific capacity throughout the cycling process. Meanwhile, the doping ensures the integrity of the crystal structure and reduces the generation of oxygen. The dual effect of coating and doping ensures more excellent cycling stability of U-NCM than that of C-NCM. S-NCM has become unusable due to the lack of Li^+ and the presence of numerous structural defects and impurity phases, exhibiting an extremely low discharge specific capacity at a rate of 0.5C. In order to verify the proposed regeneration strategy, we carried out XRD and XPS characterization on the cycled U-NCM and C-NCM (Fig. S3 and 4†). After 250 charge–discharge cycles, the splitting peak characteristics of (108) and (110) representing the layered structure of C-NCM weaken, while U-NCM still exhibits strong splitting peak characteristics. This indicates that after modification, the regenerated cathode has an enhanced ability to resist phase transition, which is mainly related to the fixation of lattice oxygen. The XPS results show that, thanks to the F–Ni bond suppressing the oxidation of Ni, the proportion of Ni^{2+} in the cycled U-NCM cathode is higher, corresponding to its excellent electrochemical performance. The electrochemical stability of cathode materials at various current densities is verified through a constant current rate test. As shown in Fig. 5c, from 0.1C to 1C, U-NCM and C-NCM exhibit similar electrochemical performance. When the current density is increased to 3C and 5C, the advantage of U-NCM gradually emerges, with its discharge specific capacity surpassing that of C-NCM. This is consistent with the characteristics of the cathode materials modified through coating and doping.[34,35]

Cyclic voltammetry (CV) curves of the cathode materials were obtained at a scanning rate of 0.1 mV s^{-1} within the voltage range of 2.5–4.5 V to verify the reversibility of the electrochemical cycling process of the materials. Fig. 5d shows the first cycle CV curves for U-NCM, S-NCM and C-NCM. Notably, the intensity of the oxidation peak for the S-NCM is quite low and not sufficiently sharp, while its reduction peak around 3.6 V is nearly invisible. It indicates that the reversibility of the redox reaction for the S-NCM is extremely low, which corresponds to its initial charge/discharge curve. Both U-NCM and C-NCM exhibit a pair of redox peaks, which are related to the reversible redox reaction of Ni^{2+}/Ni^{4+}. The reaction kinetics of the cathode material can be determined to some extent by the size of the voltage gap between the redox peaks. The voltage gap of S-NCM is the largest, reaching 464 mV, indicating that the Li/Ni mixed rows in S-NCM obstruct the Li^+ diffusion channel and negatively impact its redox reaction kinetics.[36] The voltage gap of U-NCM is 101 mV, which is lower than that of S-NCM and C-NCM (452 mV). This indicates that the regenerated cathode is modified to have optimal reaction kinetics. The electrochemical impedance spectroscopy (EIS) plots of U-NCM, S-NCM, and C-NCM presented in Fig. S15† reflect the electrical conductivity of the different samples and correspond to the results of the electrochemical performance tests described previously. In the mid- to high-frequency region of the impedance spectrum, the magnitude of the semicircle diameter correlates with the charge transfer impedance (R_{ct}) at the electrolyte–cathode interface.[8] Based on the impedance spectra and local magnification patterns of the three samples, it can be observed that U-NCM exhibits low charge transfer impedance, indicating that the ionic conductivity at the interface between the electrolyte and U-NCM is high. The result can be attributed to the Li-rich coating layer on the surface of U-NCM, which facilitates Li^+ transport, thereby enhancing the electrochemical performance of U-NCM. The highest R_{ct} of S-NCM is attributed to the presence of a thick layer of electrochemically inert disordered rock salt phase impurities on its surface, which impedes Li^+ diffusion, thereby reducing the electrochemical activity of S-NCM to some extent. To further validate the enhancement of the Li^+ transport capacity in regenerated cathodes, the Li^+ diffusion capacity of U-NCM and S-NCM was explored through the galvanostatic intermittent titration technique (GITT) test. As shown in Fig. 5e–f and S18,† the Li^+ diffusion coefficient of U-NCM is consistently higher than that of S-NCM and C-NCM, both during charging and discharging stages. In summary, it is demonstrated that the proposed regeneration strategy can not only repair used cathodes in terms of elemental content and structure but also enhance the performance of the cathode material by modifying in parallel with the regeneration process, ensuring that the regenerated cathode remains competitive compared with similar commercial cathodes.

2.3. DFT calculations of upcycled NCM

In order to investigate the mechanism by which N, F co-doping improves the electrochemical performance of regenerated NCM cathode materials, density functional theory (DFT) calculations on U-NCM, S-NCM and C-NCM were performed using the Vienna *Ab initio* Simulation Package (VASP). As shown in Fig. 6a, F atoms are doped at the O sites and N atoms are doped at the Li–O slabs. The F–Ni bond is formed between F and Ni, while the N–O bond is formed between N and O. The F–Ni bond is formed between F and Ni. According to the XRD refinement results, the quantity ratio of F to N is 2 : 1. The S-NCM is modeled by removing 39 Li atoms from the model of the C-NCM (Fig. 6b and c). The density of states (DOS) of the three groups of samples was calculated and the difference in energy gaps of the three samples was obtained, which can determine their electrical conductivity and reactivity. As shown in Fig. 6d–f, the energy gap of the U-NCM is 0.614 eV, which is lower than that of the S-NCM (1.337 eV) and the C-NCM (0.948 eV). It indicates that the conductivity of U-NCM is enhanced after co-doping with F and N elements.[37] During the electrochemical reaction process, U-NCM can rapidly transfer electrons and ions, and thus U-NCM has a higher conductivity and chemical reaction activity and can carry out the lithiation/de-lithiation reaction more rapidly, corresponding to the excellent electrochemical performance of U-NCM. In addition, N–O bonds are formed between N and O atoms, and the anchoring effect of N atoms that fixed O atoms inhibits the release of O atoms from U-NCM during electro-

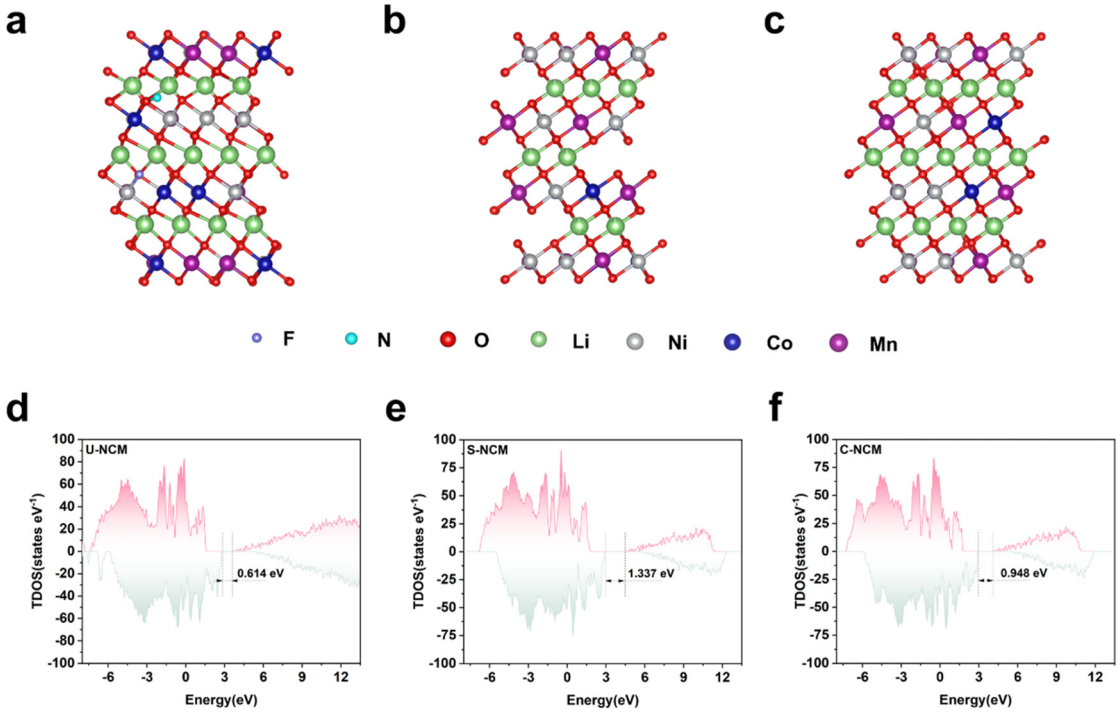

Fig. 6 The optimized structure of (a) U-NCM, (b) S-NCM and (c) C-NCM. Total density of states (TDOS) of (d) U-NCM, (e) S-NCM and (f) C-NCM.

chemical cycling, thus stabilizing the lattice structure and enhancing the cycling stability of the cathode material.[38]

3. Conclusion

In conclusion, we proposed a one-step upcycling strategy for the S-NCM cathode to achieve a dual-modification effect. By employing LiTFSI as a doping and coating agent, Li_2SO_4, Li_3N, $LiNO_3$, and LiF coating layers that facilitate Li^+ transport are formed on the surface of the upcycled cathode U-NCM, providing protection to the U-NCM from the electrolyte. Moreover, the F and N elements diffuse into the interior of the cathode material, forming F–Ni bonds and N–O bonds. The F–Ni bond inhibits the oxidation of Ni^{2+} to Ni^{3+}, thereby enhancing the regeneration efficiency of spent cathodes and diminishing the formation of harmful spinel and rock salt phases. The N–O bond binds the oxygen firmly within the lattice and stabilizes the lattice structure. The dual-modification upcycling strategy effectively repairs the spent cathodes and enhances the electrochemical performance of the regenerated cathodes. Specifically, the U-NCM has a high initial discharge specific capacity of 168.8 mAh g^{-1} at 0.1C, and a capacity retention of 77.1% after 200 cycling at a rate of 0.5C. The recycling strategy offers insights for upcycling used cathodes into cathode materials with superior performance, thereby expected to foster further advancement of the recycling industry for spent LIBs.

Conflicts of interest

There are no conflicts to declare.

Data availability

The data that support the findings of this study are available from the corresponding author upon reasonable request.

Acknowledgements

This work was supported by the Beijing Natural Science Foundation (Z240023), the Beijing Nova Program (20250484798), and the Science Fund of Shandong Laboratory of Advanced Materials and Green Manufacturing at Yantai (AMGM2024F16).

References

1 H. C. Ji, J. X. Wang, J. Ma, H. M. Cheng and G. M. Zhou, *Chem. Soc. Rev.*, 2023, **52**, 8194–8244.
2 J. Shen, M. Zhou, W. Liu, Y. Shi, W. Tang, Y. Deng, R. Liu, Y. Zuo and J. Zhang, *Energy Storage Mater.*, 2024, **74**, 103964.
3 X. Xiao, L. Wang, Y. Q. Wu, Y. Z. Song, Z. H. Chen and X. M. He, *Energy Environ. Sci.*, 2023, **16**, 2856–2868.
4 X. X. Zhang, L. Li, E. S. Fan, Q. Xue, Y. F. Bian, F. Wu and R. J. Chen, *Chem. Soc. Rev.*, 2018, **47**, 7239–7302.

5 J. Neumann, M. Petranikova, M. Meeus, J. D. Gamarra, R. Younesi, M. Winter and S. Nowak, *Adv. Energy Mater.*, 2022, **12**, 2102917.
6 M. Fan, X. H. Meng, H. Guo, S. Xin, X. Chang, K. C. Jiang, J. C. Chen, Q. Meng and Y. G. Guo, *Adv. Mater.*, 2024, **36**, 2405238.
7 X. Yu, S. Yu, J. Lin, V. Gupta, H. Gao, W. Li, M. Appleberry, P. Liu and Z. Chen, *Adv. Mater.*, 2024, **36**, 2408463.
8 Z. Qin, Y. Zhang, W. Luo, T. Zhang, T. Wang, L. Ni, H. Wang, N. Zhang, X. Liu and J. Zhou, *Angew. Chem., Int. Ed.*, 2023, **62**, e202218672.
9 J. Shen, M. M. Zhou, W. H. Tang, Q. R. Huang, H. C. Pi, W. Liu, R. P. Liu and L. Li, *Nano Energy*, 2025, **136**, 110741.
10 M. Fan, Q. Meng, X. Chang, C. F. Gu, X. H. Meng, Y. X. Yin, H. Li, L. J. Wan and Y. G. Guo, *Adv. Energy Mater.*, 2022, **12**, 2103630.
11 D. Yang, Z. Fang, Y. Ji, Y. Yang, J. Hou, Z. Zhang, W. Du, X. Qi, Z. Zhu and R. Zhang, *Angew. Chem., Int. Ed.*, 2024, **63**, e202409929.
12 J. Wang, J. Ma, K. Jia, Z. Liang, G. Ji, Y. Zhao, B. Li, G. Zhou and H.-M. Cheng, *ACS Energy Lett.*, 2022, **7**, 2816–2824.
13 Y.-C. Yin, C. Li, X. Hu, D. Zuo, L. Yang, L. Zhou, J. Yang and J. Wan, *ACS Energy Lett.*, 2023, **8**, 3005–3012.
14 H. J. Guo, Y. Sun, Y. Zhao, G. X. Liu, Y. X. Song, J. Wan, K. C. Jiang, Y. G. Guo, X. Sun and R. Wen, *Angew. Chem., Int. Ed.*, 2022, **61**, e202211626.
15 J. Liu, X. Hu, S. Qi, Y. Ren, Y. Li and J. Ma, *InfoMat*, 2024, **6**, e12507.
16 Z. Yang, C. Xing, L. Chen, S. Tao, Y. Zhang, G. Wang, P. Yang, J. Zhou, C. Zhang and J. Chen, *Adv. Funct. Mater.*, 2025, **35**, 2409737.
17 X. Li, A. Gao, Z. Tang, F. Meng, T. Shang, S. Guo, J. Ding, Y. Luo, D. Xiao and X. Wang, *Adv. Funct. Mater.*, 2021, **31**, 2010291.
18 J. Choi, D. Darbar, M. Chen, X. Huang, G. Qi, L. Wang and J.-H. Kim, *ACS Appl. Energy Mater.*, 2024, **7**, 6920–6928.
19 L. Liu, M. Li, L. Chu, B. Jiang, R. Lin, X. Zhu and G. Cao, *Prog. Mater. Sci.*, 2020, **111**, 100655.
20 M. Zhou, J. Shen, Y. Zuo, R. Liu, J. Zhao and G. Zhou, *Angew. Chem., Int. Ed.*, 2024, **64**, e202414484.
21 F. Guo, Y. Hu, L. Qiu, Y. Jiang, Y. Deng, J. Zhou, Z. Zheng, Y. Liu, Y. Sun and Z. Wu, *J. Mater. Chem. A*, 2023, **11**, 11819–11830.
22 X. Liu, R. H. Wang, S. Q. Liu, J. H. Pu, H. G. Xie, M. L. Wu, D. M. Liu, Y. Li and J. W. Liu, *Adv. Energy Mater.*, 2023, **13**, 2302957.
23 L. S. Ni, H. Y. Chen, W. T. Deng, B. W. Wang, J. Chen, Y. Mei, G. Q. Zou, H. S. Hou, R. Guo, J. Y. Xie and X. B. Ji, *Adv. Energy Mater.*, 2022, **12**, 2103757.
24 Z. Qin, Z. Wen, Y. Xu, Z. Zheng, M. Bai, N. Zhang, C. Jia, H. B. Wu and G. Chen, *Small*, 2022, **18**, 2106719.
25 N. Z. Zheng, H. C. Ji, J. X. Wang, M. T. Zhang, L. L. Wei, R. Y. Shi, K. Jia, X. R. Wu, X. Xiao, Z. F. Zhuang, B. Li, H. M. Cheng and G. M. Zhou, *J. Am. Chem. Soc.*, 2024, **146**, 27819–27829.
26 Q. R. Huang, X. D. Zhang, F. Wu, R. J. Chen and L. Li, *Energy Storage Mater.*, 2023, **63**, 103050.
27 X. L. Yu, S. C. Yu, J. Lin, V. Gupta, H. P. Gao, W. K. Li, M. Appleberry, P. Liu and Z. Chen, *Adv. Mater.*, 2024, **36**, 2408463.
28 W. Liu, P. Oh, X. Liu, M. J. Lee, W. Cho, S. Chae, Y. Kim and J. Cho, *Angew. Chem., Int. Ed.*, 2015, **54**, 4440–4457.
29 Z. Z. Liu, H. M. Li, M. M. Han, L. Fang, Z. Fu, H. M. Zhang, G. Z. Wang and Y. X. Zhang, *Adv. Energy Mater.*, 2023, **13**, 2302058.
30 L. Hong, Y. Zhang, P. Mei, B. Ai, Y. Zhang, C. Zhou, X. Bao and W. Zhang, *Angew. Chem., Int. Ed.*, 2024, e202409069, DOI: **10.1002/anie.202409069**.
31 X. Y. Zhang, M. M. Jia, Q. P. Zhang, N. A. Zhang, X. K. Wu, S. T. Qi and L. Zhang, *Chem. Eng. J.*, 2022, **448**, 137743.
32 C. M. Subramaniyam, H. Celio, K. Shiva, H. C. Gao, J. B. Goodneough, H. K. Liu and S. X. Dou, *Sustainable Energy Fuels*, 2017, **1**, 1292–1298.
33 J. X. Wang, K. Jia, J. Ma, Z. Liang, Z. F. Zhuang, Y. Zhao, B. H. Li, G. M. Zhou and H. M. Cheng, *Nat. Sustain.*, 2023, **6**, 797–805.
34 W. Liu, X. F. Li, D. B. Xiong, Y. C. Hao, J. W. Li, H. R. Kou, B. Yan, D. J. Li, S. G. Lu, A. Koo, K. Adair and X. L. Sun, *Nano Energy*, 2018, **44**, 111–120.
35 K. Jia, J. Wang, J. Ma, Z. Liang, Z. Zhuang, G. Ji, R. Gao, Z. Piao, C. Li and G. Zhou, *Nano Lett.*, 2022, **22**, 8372–8380.
36 K. Jia, J. X. Wang, Z. F. Zhuang, Z. H. Piao, M. T. Zhang, Z. Liang, G. J. Ji, J. Ma, H. C. Ji, W. J. Yao, G. M. Zhou and H. M. Cheng, *J. Am. Chem. Soc.*, 2023, **145**, 7288–7300.
37 M. M. Zhou, J. Shen, Y. Duan, Y. Z. Zuo, Z. W. Xing and R. P. Liu, *Energy Storage Mater.*, 2024, **67**, 103250.
38 Z. Liu, H. Li, M. Han, L. Fang, Z. Fu, H. Zhang, G. Wang and Y. Zhang, *Adv. Energy Mater.*, 2023, **13**, 2302058.